Sequential Structural Changes of *Escherichia coli* Thioesterase/Protease I in the Serial Formation of Michaelis and Tetrahedral Complexes with Diethyl *p*-Nitrophenyl Phosphate†

Sergiy I. Tyukhtenko,‡ Alexandra V. Litvinchuk,‡ Chi-Fon Chang,‡ Yu-Chih Lo,§ Shin-Jye Lee,‡ Jei-Fu Shaw,|| Yen-Chywan Liaw,§ and Tai-Huang Huang*,‡,⊥

Institute of Biomedical Sciences, Institute of Botany, and Institute of Molecular Biology, Academia Sinica, Nankang, Taipei, Taiwan 11529, Republic of China, and Department of Physics, National Taiwan Normal University, Taipei, Taiwan, Republic of China

Received November 26, 2002; Revised Manuscript Received May 7, 2003

ABSTRACT: *Escherichia coli* thioesterase/protease I (TEP-I) belongs to a new subclass of lipolytic enzymes of the serine hydrolase superfamily. Here we report the first direct NMR observation of the formation of the Michaelis complex (MC) between TEP-I and diethyl *p*-nitrophenyl phosphate (DENP), an active site directed inhibitor of serine protease, and its subsequent conversion to the tetrahedral complex (TC). NMR, ESI-MS, and kinetic data showed that DENP binds to TEP-I in a two-step process, a fast formation of MC followed by a slow conversion to TC. NMR chemical shift perturbation further revealed that perturbations were confined mainly to four conserved segments comprising the active site. Comparable magnitudes of chemical shift perturbations were detected in both steps. The largest chemical shift perturbation occurred around the catalytic Ser^{10}. In MC, the conformation of the mobile Ser^{10} was stabilized, and its amide resonance became observable. From the large chemical shift perturbation upon conversion from MC to TC, we propose that the amide protons of Ser^{10} and Gly^{44} serve as the oxyanion hole proton donors that stabilize the tetrahedral adduct. The pattern of residues perturbed in both steps suggests a sequential, stepwise structural change upon binding of DENP. The present study also demonstrates the important catalytic roles of conserved residues in the SGNH family of proteins.

Serine proteases are among the most studied enzymes based on their roles as model enzymes for the study of the mechanism of enzyme catalysis as well as the medical implication of their inhibition. This class of enzymes employs a "catalytic triad" of serine, histidine, and aspartic acid as catalytic residues. The general catalytic sequence of serine proteases includes formation of a noncovalent Michaelis complex. Nucleophilic attack by the active site Ser residue of the peptide carbonyl group results in the formation of a tetrahedral oxyanion intermediate, which subsequently releases the C-terminal product fragment to form the acyl-enzyme at the Ser residue. In the second deacylation reaction, hydrolytic attack by a water molecule on the ester carbonyl group leads to the formation of the second tetrahedral intermediate, which collapses to yield an N-terminal product fragment and the restoration of free enzyme. Formation of multiple intermediates with lower activation energy than the overall uncatalyzed step constitutes the main theme of the transition state theory for enzyme catalysis (*1*−*5*). Therefore, to understand the mechanism of catalysis for the enzyme, it is necessary to determine the structure and define the source of the binding power of the enzyme for all intermediate states. However, the lifetimes of transition states are very short (about 10^{-13} s) and are very hard to characterize. In 1969, Wolfenden recognized that transition state analogues (TSA),[1] molecules that mimic the transition state of an enzyme-catalyzed reaction, should bind tightly to the enzyme and could be used as a model of the transition state (*6*). Use of TSAs has provided considerable insight into the interactions between TSA and the enzyme and the structures of the intermediate species (*7*). Recently, the crystal structures of the acyl-enzyme and the tetrahedral intermediate, trapped at cryotemperatures, of pancreatic elastase in complex with the heptapeptide human β-casomorphin 7 have been reported (*8*−*10*).

† This work was supported by Grant 91-2113-M-001-038 (T.-H.H.) from the National Science Council of the Republic of China. The NMR spectra were obtained at the High-Field Biomacromolecular NMR Core Facility, and the ESI-MS data were obtained at the Core Facility for Proteomic Research, National Program for Genomic Medicine, Taiwan, Republic of China.

* Address correspondence to this author at the Institute of Biomedical Sciences, Academia Sinica. Tel: (886)-2-2652-3036. Fax: 2-2788-7641. E-mail: bmthh@ibms.sinica.edu.tw.

‡ Institute of Biomedical Sciences, Academia Sinica.

§ Institute of Molecular Biology, Academia Sinica.

|| Institute of Botany, Academia Sinica.

⊥ Department of Physics, National Taiwan Normal University.

[1] Abbreviations: AURELIA, *au*tomated *re*sonance *li*ne *a*ssignment; DENP, diethyl *p*-nitrophenyl phosphate; DEP, diethyl phosphate; DSS, 2,2-dimethyl-2-silapentane-5-sulfonate; ESI-MS, electrospray ionization mass spectrometry; HSQC, heteronuclear single-quantum correlated spectroscopy; L-NBTNPE, *N*-carbobenzoxy-L-tyrosine *p*-nitrophenyl ester; MC, Michaelis complex; T, tesla (SI unit of magnetic field); TSA, transition state analogue; TC, tetrahedral complex; TEP-I, *Escherichia coli* thioesterase/protease I.

10.1021/bi027246w CCC: $25.00
Published on Web 06/17/2003

Escherichia coli thioesterase/protease I is a 182 amino acid single peptide protein (*11*−*13*). It has been classified as a member of a new subclass of the lipolytic enzymes with diverse substrate specificity and regiospecificity (*14*, *15*). Recently, a subgroup of this new hydrolase family has been further classified as the SGNH-hydrolase due to the presence of four strictly conserved residues: serine (S), glycine (G), asparagine (N), and histidine (H) in four conserved blocks (*16*, *17*). Each of the four residues plays a central role in the catalytic function. Block I contains the serine nucleophile and is positioned in a type I β turn at the carboxyl end of β strand 1. The amide proton of this serine residue also serves as a hydrogen bond donor to the oxyanion hole. Block II contains the glycine residue which is positioned after the β strand 2 and whose amide proton serves as a hydrogen bond donor to the oxyanion hole. Block III contains the asparagine positioned after β strand 3. The side chain H^{δ} serves as the proton donor to the oxyanion hole. Block V contains the catalytic aspartic acid and histidine residues and is positioned at the loop after the last β strand in the central sheet. Sequence comparison has shown that all of these features are strikingly conserved in TEP-I. The corresponding four conserved residues are Ser^{10}, Gly^{44}, Asn^{73}, and His^{157}. Thus, TEP-I is likely to be a member of this new SGNH-hydrolase subfamily. We have applied heteronuclear multidimensional NMR techniques to determine the structure and dynamics of TEP-I (*18*, *19*). Our results show that TEP-I consists of a four-strand parallel β-sheet and seven α-helices. The folding topology is of the $\alpha/\beta/\alpha$ type. A recent 1.95 Å resolution crystal structure further identified Ser^{10}, Asp^{154}, and His^{157} as the catalytic triad residues (Lo and Liaw, unpublished results; PDB code 1JRL). The structural features fit well to the new hydrolase family, the SGNH-hydrolase family (*16*). Our NMR relaxation studies have further shown that TEP-I possesses a rigid core structure comprising the β sheet and α helices. Built on the rigid frame is a highly flexible binding pocket, comprising loops 1, 3, 5, 7, and 9 (*19*). To gain a deeper understanding of the catalytic mechanism of TEP-I, we have studied its interaction with diethyl *p*-nitrophenyl phosphate (DENP), an active site directed inhibitor for serine proteases (*20*, *21*). The PO group of DENP reacts with the active site serine to form a stable tetrahedral complex. The binding of DENP to TEP-I is very slow and irreversible, permitting us to characterize the structural changes involved in the formation of the DENP/TEP-I Michaelis complex and its subsequent conversion to the tetrahedral complex. Our results provide detailed information on the structural changes leading to phosphorylation of the enzyme, mimicking the formation of the covalent enzyme/substrate complex. As far as we know, this is the first direct NMR observation of the Michaelis complex formation and its conversion to the tetrahedral complex of serine proteases.

MATERIALS AND METHODS

Protein Expression and Purification. The procedures for expressing and purifying *E. coli* thioesterase/protease I have been described previously (*14*). Briefly, the BL21(DE3) strain of *E. coli* was transformed with an expression plasmid (pET-thio) carrying the *tes*A/*ape*A gene under the control of the T7 promoter. To facilitate protein expression and purification, the expressed protein contains an extra methionine residue at the N-terminus and a leucine and a glutamic acid and six histidine residues at the C-terminus. The full length of the expressed protein therefore contains 191 amino acids. Here we will use the wild-type protein sequence to number the amino acid sequence. The protein was purified with Ni-NTA affinity chromatography, and the purity of the protein was found to be greater than 95% pure, based on the Coomassie blue stained gel. The N-terminal methionine and the C-terminal histidine tag were not cleaved after the purification. The protein activity was found to be almost identical to that of the wild-type protein (*22*). The uniform ^{15}N-labeling was achieved by growing the *E. coli* cells in M9 medium with $^{15}NH_4Cl$ as the only nitrogen source (*18*). The protein concentration was determined spectrophotometrically using a molar extinction coefficient, $\epsilon_{280} = 34850\ M^{-1}\ cm^{-1}$ (*23*). The typical protein yield was about 10−15 mg/L for cells grown in M9 medium. To obtain protein samples with ^{15}N label at specific amino acids, cells were grown in M9 medium, supplemented with 2 g/L unlabeled glucose and 1 g/L unlabeled NH_4Cl. After cells had grown to an OD of 0.8, the desired amino acid (^{15}N-labeled) was added, together with IPTG (1 mM). The amount of labeled amino acid added to each preparation was 600 mg/L for alanine, 60 mg/L for leucine, and 60 mg/L for phenylalanine.

Esterase Activity Assay. The assay mixture (1 mL) contains between 1.3 and 7.9×10^{-4} M substrate (*p*-nitrophenyl butyrate) in 50 mM sodium phosphate buffer and 2.1% Triton X-100, pH 7.0. The reaction was carried out at 37 °C and initiated by the addition of enzyme or its inhibitor complex (final concentration of enzyme 1.64×10^{-8} M) and terminated by the addition of 0.4 mL of acetone. Initial rates were estimated by measuring the amount of *p*-nitrophenol formation, which was monitored at 346 nm ($\epsilon_{max} = 925\ M^{-1}\ cm^{-1}$) (*24*).

Protease Activity. The assay mixture contained the substrate, *N*-carbobenzoxy-L-tyrosine *p*-nitrophenyl ester (L-NBTNPE) (dissolved in freshly made dioxane solution), and the enzyme or its inhibitor complex (final enzyme concentration 1.64×10^{-8} M) in 50 mM phosphate buffer, pH 7.0. The enzymatic activity was estimated spectrophotometrically at 25 °C (*12*).

Thioesterase Activity. The assay is based on enzymatic release of coenzyme A (CoA) as measured by reduction of 5,5-dithiobis(2-nitrobenzoic acid) (DTNB). The reduction of DTNB was measured by following an increase in absorbance at 412 nm for 2−6 min with a molar extinction coefficient of $13600\ M^{-1}\ cm^{-1}$. The assay mixture contained 0.1 mM DTNB, 80 μg/mL bovine serum albumin, and 14 μM palmitoyl-CoA in 50 mM phosphate buffer, pH 7.0. The final enzyme concentration was 3.28×10^{-8} M (*25*).

Mass Spectrometry. Electrospray ionization mass spectrometry (ESI-MS) experiments were carried out on a Finnigan LCQ Deca ion trap mass spectrometer (ThermoFinnigan, San Jose, CA) with an electrospray ionization interface. The ESI source was operated in positive ion mode. Sample solution was infused using an HPLC pump with loop injection. ESI operation conditions involved a spray voltage of 4.5 kV, a heated capillary temperature of 160 °C, and flow rate of 5 μL/min. The mass spectrometer was operated in full-scan profile mode, with the scan range from *m*/*z* 150 to *m*/*z* 2000. Xcalibur (version 1.3, ThermoFinnigan) and BioWorks 3.0 software packages were used for data acquisi-

tion and analysis and in reconstruction of the molecular weight from the spectra. NMR spectra of samples for ESI-MS analysis were taken to confirm their complex states prior to mass analysis.

NMR Experiments. NMR samples were prepared by adding aliquots of a concentrated solution of DENP (Sigma) in water to a solution of the ^{15}N-labeled enzyme (0.4−0.8 mM) in 50 mM sodium phosphate buffer at desired pHs. NMR spectra were recorded on a Bruker AVANCE 600 spectrometer using a 5 mm inverse triple-resonance (^{1}H/^{13}C/^{15}N) probe head fitted with self-shielded *X*-, *Y*-, and *Z*-gradient coils. Two-dimensional ^{1}H−^{15}N-HSQC spectra were recorded at 310 or 285 K using the WATERGATE sequence for solvent signal suppression (*26*). The spectral widths used were 6.5 ppm for ^{1}H and 46 ppm for ^{15}N. The proton carrier frequency was placed on the water peak during the pulse sequence and was shifted to 8 ppm just before data acquisition. The nitrogen carrier frequency was set to 115 ppm. The data matrix contains 1024 complex points in the ^{1}H dimension and 128 increments in the ^{15}N dimension. Data were processed using XWINNMR software (Bruker AG, Karlsruhe, Germany) on a UNIX-based Silicon Graphics O2 workstation. The proton chemical shift values were referenced to DSS at 0 ppm (*27*). The ^{15}N chemical shift values were indirectly referenced using the following consensus Ξ ratio of 0.101329118 for ^{15}N/^{1}H (*28*). The AURELIA program was employed for data analysis and peak picking (*29*).

RESULTS

pH Profile of Phosphorylation of TEP-I by DENP. Catalysis by TEP-I involves acylation and deacylation of Ser^{10}, both of which are sensitive to pH because they depend on the state of ionization of the catalytic His^{157} residue. Figure 1a shows the pH-dependent protease activity of TEP-I. The activity of TEP-I showed a maximum at pH ∼8.0 with a drop in activity at both higher and lower pHs. The loss of activity of TEP-I at low pH is presumably due to the protonation of the catalytic His^{157}, whose pK_a was estimated to be ∼6.8 (*30*). The loss of activity at higher pH is likely to be the result of structural changes at high pH.

DENP is a known active site directed inhibitor for serine proteases (*20*, *21*). The loss of enzyme activity of TEP-I in the presence of DENP was examined by preincubating the enzyme with DENP and assayed according to previously established procedures (*12*, *24*, *25*). DENP was found to irreversibly inhibit both the protease and thioesterase activities of TEP-I (data not shown). As a mechanism-based inhibitor, the inhibitory activity of DENP should also display similar pH dependence. Inhibition of the enzymatic activity of TEP-I by DENP involves phosphorylation of the catalytic Ser^{10} residue. Thus, the rate of inhibition is directly proportional to the rate of *p*-nitrophenol release. Figure 1b shows the effect of pH on the rate of phosphorylation of TEP-I, measured by the amount of *p*-nitrophenol released after 90 min of incubation of DENP in the enzyme solution. The pH profile of DENP inhibition is indeed similar to that of the protease activity profile. The sharp decrease on the rate of release of *p*-nitrophenol at low pH permits the trapping of the Michaelis complex for structural characterization. However, to keep our study more functionally relevant,

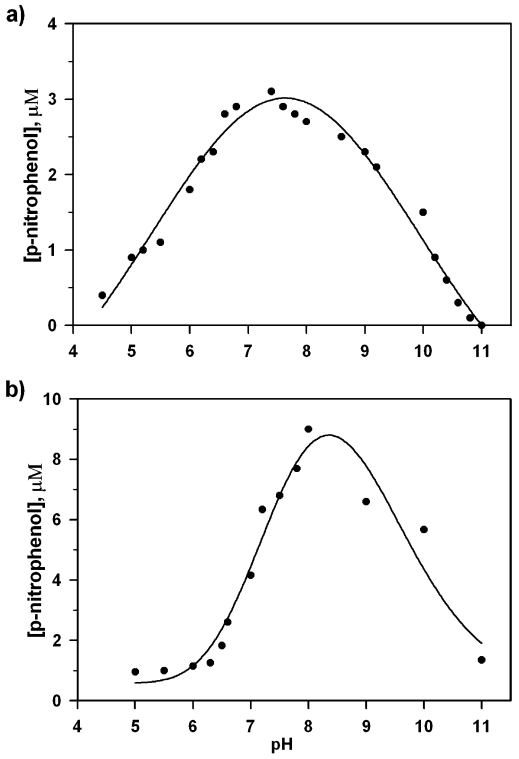

FIGURE 1: (a) Effect of pH on protease activity of TEP-I. The concentration of reagents was [TEP-I] = 32 nM and [L-NBTNPE] = 20 μM. Protease activities were expressed as the concentration of *p*-nitrophenol released at 20 s after the addition of enzyme to the assay mixture. (b) Effect of pH on phosphorylation of TEP-I by DENP. The rates of the phosphorylation reaction were reported as the amount of *p*-nitrophenol released at 90 min after the addition of DENP to the enzyme. Concentrations of reagents were [TEP-I] = 11 μM and [DENP] = 1.1 mM. The concentration of released *p*-nitrophenol in both cases was measured by an increase of absorbance at 346 nm. All measurements were made at 25 °C at the desired pH.

we conducted all studies at pH 6.0 but used low temperature to prolong the lifetime of the intermediate species.

Kinetics of the Release of p-Nitrophenolate from the DENP/TEP-I Complex. Scheme 1 depicts the mechanism of inhibition of TEP-I by DENP and the possible formation of "aged" adduct (*21*, *31*). Following the formation of the Michaelis complex the mechanism-based inhibitor DENP (structure I) forms a covalent tetrahedral complex (TC, structure II) with the active site Ser^{10}, with the departure of *p*-nitrophenolate. The TC can further dissociate into a phosphodiester anion (structure III) with the departure of the ethyl group. The rate of inhibition of TEP-I by DENP can be followed by determining the rate of release of *p*-nitrophenolate, which can be determined spectrophotometrically using an extinction coefficient of ϵ_{400nm} = 8000 M^{-1} cm^{-1}. Figure 2A shows the changes in absorbance after TEP-I was mixed with various molar ratios of DENP at pH 7.0, 20 °C. Figure 2B shows the double-reciprocal Lineweaver−Burk plot of the initial rate of *p*-nitrophenolate release versus inhibitor concentration. From the intercepts of this curve with *x*- and *y*-axes the maximum velocity, V_{max}, and Michaelis constant, K_m, were determined to be V_{max} = 0.33 ± 0.08 μM min^{-1} and K_m = 0.73 ± 0.06 mM.

NMR Evidence for the Formation of Long-Lived Intermediate Species. TEP-I is a well-behaved protein with high pH and temperature stability. The ^{15}N-HSQC spectrum of

Scheme 1

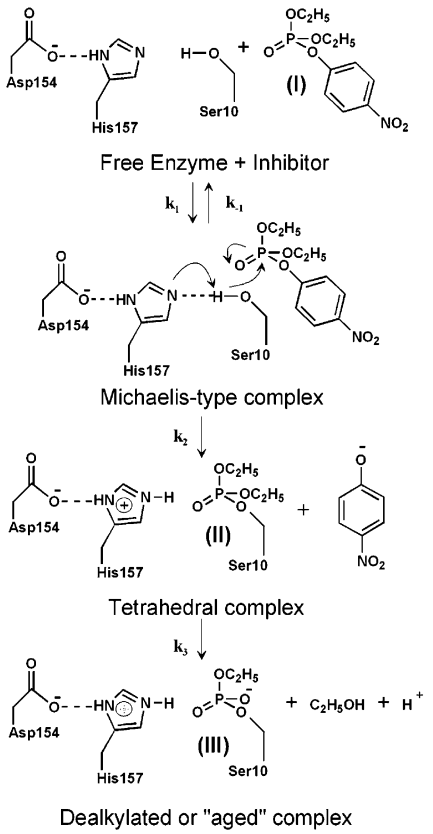

TEP-I contains well-resolved resonances that have been fully assigned (*18*). Figure 3 shows portions of the ^{15}N-HSQC spectra of DENP/[U-^{15}N]TEP-I complexes at conditions under which various species can be detected. Addition of DENP resulted in the appearance of new resonances with a concomitant decrease in intensities corresponding to free enzyme. We observed two sets of new resonances: (1) transient resonances that appeared only for a short period of time after the addition of DENP and then disappeared again after prolonged exposure to the inhibitor and (2) resonances that appeared at a later time. Figure 3a shows the spectrum, obtained at 310 K, of [U-^{15}N]TEP-I after being incubated with a 2 times excess of DENP at 310 K for 3 h at pH 6.0. Upward thick arrows mark the resonances corresponding to intermediate species. Curved arrows trace the time sequence of the evolution of the resonances, corresponding to conversion of free TEP-I to the intermediate species and, subsequently, to the final complex. At the proper DENP molar ratio and with adjustment of pH and temperature conditions, it is possible to obtain spectra containing only the intermediate species and the final complex (Figure 3b), only the intermediate (red spectrum in Figure 3c), or only the final complex (red spectrum in Figure 3d). In general, formation of the intermediate species is rapid, but the conversion from the intermediate species to the final complex is slow. Low pH and low temperature retard the conversion of the intermediate species to the final complex.

Identity of the Intermediate Species. It is known that organophosphorus inhibitors initially phosphorylate the active site Ser residue in serine proteases to form stable tetrahedral adducts (*20*). The tetrahedral adducts can undergo further postinhibitory reactions, including dealkylation ("aging") (*21*, *31*, *32*). As depicted in Scheme 1, the enzyme can potentially

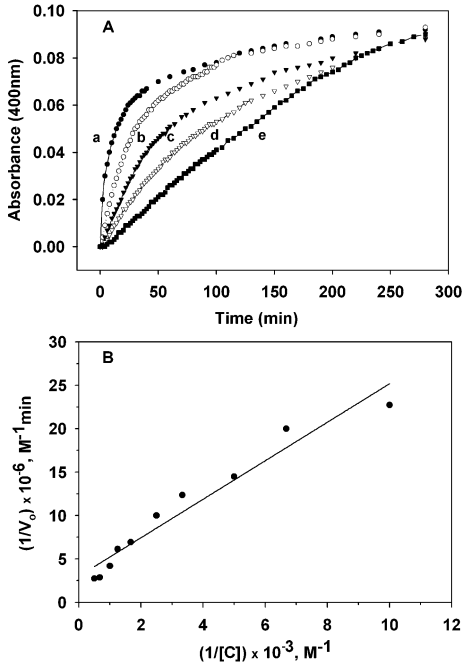

FIGURE 2: (A) Time course of *p*-nitrophenolate release from the TEP-I/DENP complex in 50 mM phosphate buffer, pH 7 at 20 °C. The reaction was initiated by the addition of enzyme to the DENP solution, and the release of *p*-nitrophenolate was monitored spectrophotometrically by measuring the increase in absorbance at 400 nm. The enzyme concentration in the cuvette was 10 μM. Molar ratios of DENP/TEP-I are (a) 150, (b) 100, (c) 60, (d) 40, and (e) 10. (B) Lineweaver−Burk plot of the inhibition of TEP-I by DENP. The initial velocities were determined from the initial slopes of the curves in (A) using an extinction coefficient of $\epsilon_{400nm} = 8000$ M^{-1} cm^{-1}. The straight line is the best fit to the data points.

exist in four possible states: (i) the free enzyme,; (ii) the enzyme/DENP Michaelis complex (MC) with no covalent bond formation between the enzyme and DENP, (iii) the enzyme−inhibitor tetrahedral complex (TC) with the inhibitor covalently bonded to Ser^{10} as a phosphotriester, and (iv) the aged enzyme−inhibitor complex with the inhibitor bonded to Ser^{10} as a phosphodiester anion. To determine the identities of the intermediate species and the final species observed in our spectra, we performed the following experiments:

(i) Activity Assay. As a mechanism-based inhibitor DENP competes with substrate in interacting with TEP-I. Scheme 2 illustrates the competition between inhibitor IX (X is a leaving group) and substrate S for binding to enzyme E. If DENP exists as a noncovalent Michaelis complex, it is possible for the substrate to compete with DENP for TEP-I, and the Michaelis complex will be active. On the other hand, if DENP is covalently bound to TEP-I, the enzyme will be inactive. Thus, by measuring the enzyme activity it should be possible to determine whether the TEP-I/DENP complex is in the Michaelis complex or in the covalent complex. Small aliquots of free enzyme sample and samples at various times after addition of DENP were removed from the NMR tube for activity assay at pH 7.0, 20 °C. ^{15}N-HSQC spectra were taken at 12 °C to follow enzyme conversion from free enzyme to the intermediate species and, subsequently, to the final complex. As expected, free enzyme (Figure 4A, trace a) is the most active one while the final complex (Figure

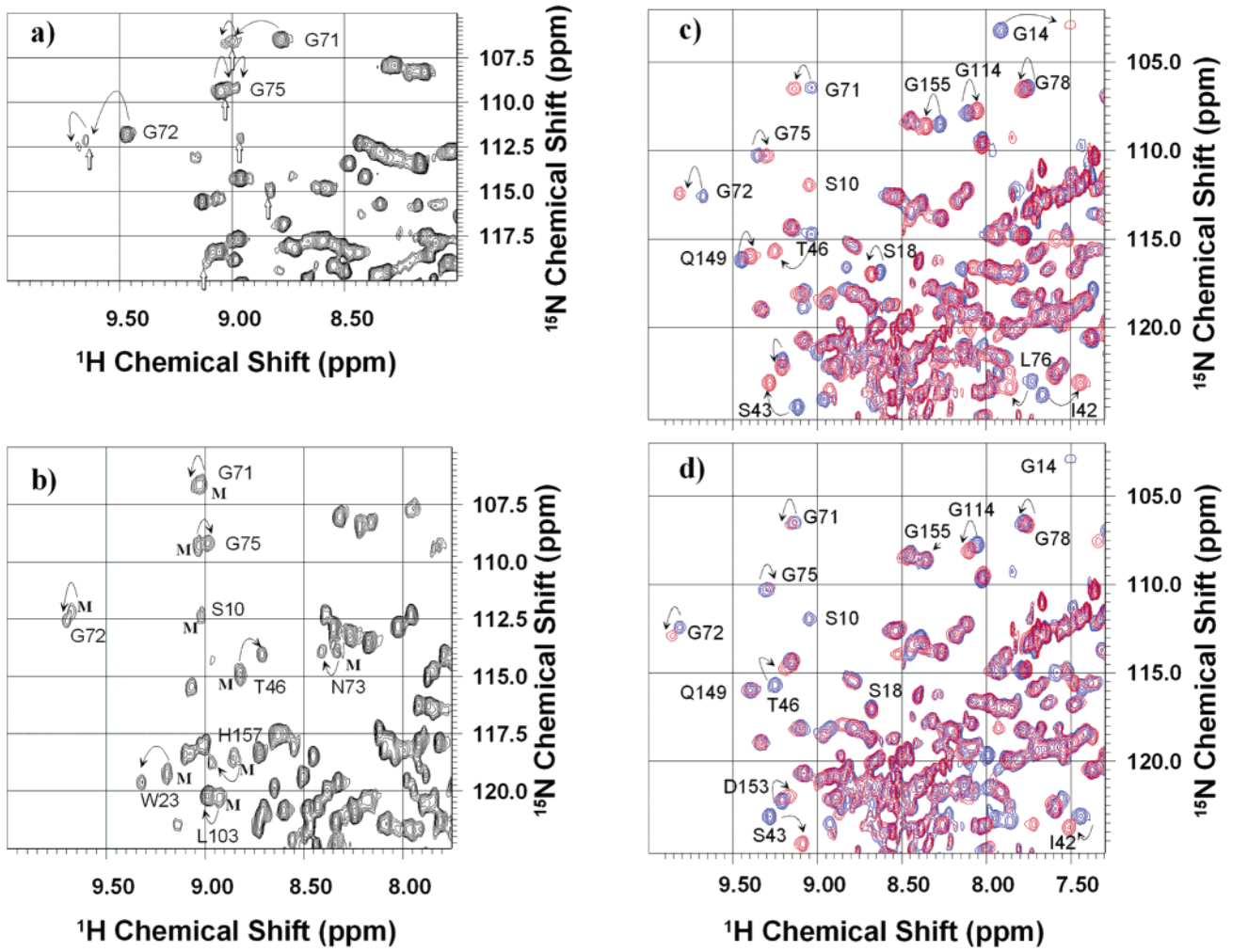

FIGURE 3: Selected regions of a set of ^{15}N-HSQC spectra of [U-^{15}N]TEP-I/DENP complexes obtained at 310 K (a and b) or 285 K (c and d) at pH 6.0 (a, c, and d) or pH 7.0 (b). [TEP-I] = 0.5 mM. (a) [DENP]/[TEP-I] = 2:1. Incubation time = 3 h at 310 K. Straight arrows indicate peaks due to the intermediate species. Curved arrows indicate evolution with time of the corresponding peaks from the free enzyme to the Michaelis complex and, subsequently, to a tetrahedral complex. (b) [DENP]/[TEP-I] = 4:1. Incubation time = 3 h at 310 K. This spectrum contains only peaks corresponding to the Michaelis complex and tetrahedral complex. Arrows connect peaks from the Michaelis complex (M) to TC. (c) Superposition of the spectra of a free enzyme (blue) and a sample containing only the Michaelis complex (red). The sample which contains only the Michaelis complex was obtained by incubating TEP-I with a 10 times excess of DENP at room temperature for 5 min. (d) Superposition of spectra of the Michaelis complex (blue) and the tetrahedral complex (red). The sample which contains only the tetrahedral complex was obtained by equilibrating the sample in (c) at 310 K for over 10 h.

Scheme 2

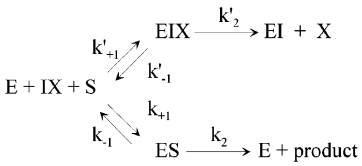

4A, trace e) is inactive. An enzyme which exists only in the intermediate species has reduced initial velocity compared to the free enzyme (Figure 4A, trace b), presumably limited by the slow dissociation of DENP from the enzyme. As more of the intermediate species converts to the final complex, the initial velocity also drops proportionally (Figure 4A, traces c and d). In the presence of a large excess of DENP all enzyme molecules exist in the Michaelis complex with DENP, and the amount of the Michaelis complex decreases exponentially with time constant equals k_2. Thus, the enzyme initial velocity, v_0, also drops exponentially. Figure 4B shows a plot of v_0 vs preincubation time of TEP-I with DENP at 37 °C, pH 6.0. The insert in Figure 4B shows a plot of ln v_0 versus preincubation time, showing a good linear relationship between ln v_0 and preincubation time. The slope of the straight line gives $k_2 = (9.6 \pm 0.4) \times 10^{-3}$ min^{-1} at 37 °C at pH 6.0. Thus, this set of data supports the assignment of the intermediate species to the noncovalent TEP-I/DENP Michaelis complex and the final complex to the inactive tetrahedral complex. However, this experiment cannot distinguish whether the inhibitor in the final complex exists as the phosphotriester (II) or the phosphodiester anion (III).

(ii) Electrospray Ionization Mass Spectrometry (ESI-MS). Figure 5 shows the ESI-MS results of two sets of samples: (a) free [U-^{15}N]TEP-I and (b) the [U-^{15}N]TEP-I/DENP complex where only resonances corresponding to the final complex were observed. The results showed a single species of mass 21790 ± 3 Da for the free enzyme and a single peak of mass 21930 ± 3 Da for the sample containing only the final complex. Masses of various DENP derivatives are 275, 137, and 108 Da for free DENP, the DENP phosphotriester form with *p*-nitrophenolate released (diethyl phosphate, DEP), and DENP in phosphodiester anionic form with

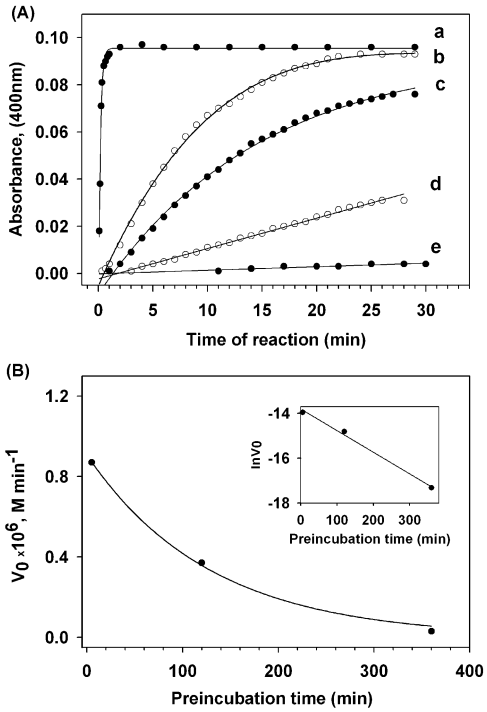

FIGURE 4: (A) Remaining enzymatic activity of TEP-I after the enzyme was preincubated with DENP at pH 6.1, 310 K, for the specified time. Trace a was determined with the pure enzyme while traces b−e were determined with the DENP-bound enzyme withdrawn from the NMR tube after the ^{15}N-HSQC spectra shown in Figure 3 were recorded. The states of TEP-I in traces b−e correspond to the pure intermediate state, predominantly in the intermediate state (2 h incubation), predominantly in the final state (6 h of incubation), and final state (2 days of incubation) for traces b, c, d, and e, respectively. The reaction mixture in the cuvette contained [TEP-I] = 1.64×10^{-7} M and [L-NBTNPE] = 2×10^{-5} M in 50 mM phosphate, pH 7.0 at 20 °C. (B) Time course of inhibition. The initial velocities were determined from the initial slopes of traces b−d shown in panel A. Data points for the pure enzyme (trace a) and final complex (trace e) were not included. The time course of ln v_0 is shown in the insert.

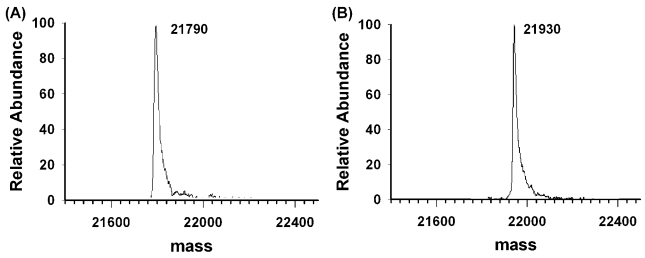

FIGURE 5: Reconstructed ESI-MS spectra of the pure enzyme (A) and the TEP-I/DENP complex (B) in the final state.

further release of the ethyl group, respectively. The present ESI-MS data clearly demonstrate that in the final complex the inhibitor exists as the phosphotriester, not the phosphodiester anion. Thus, no further release of the ethyl group occurred even after prolonged exposure of the TEP-I/DENP complex. The result of the sample which contains only the intermediate resonances is less conclusive. Two peaks at 21790 and 21927 Da were observed for this sample, suggesting that under the experimental conditions for obtaining the ESI-MS spectrum the sample has changed to either free form or the tetrahedral final form. It is known that detection of the noncovalent enzyme complex in ESI-MS is difficult due to dissociation in the gas phase (*33*). The high

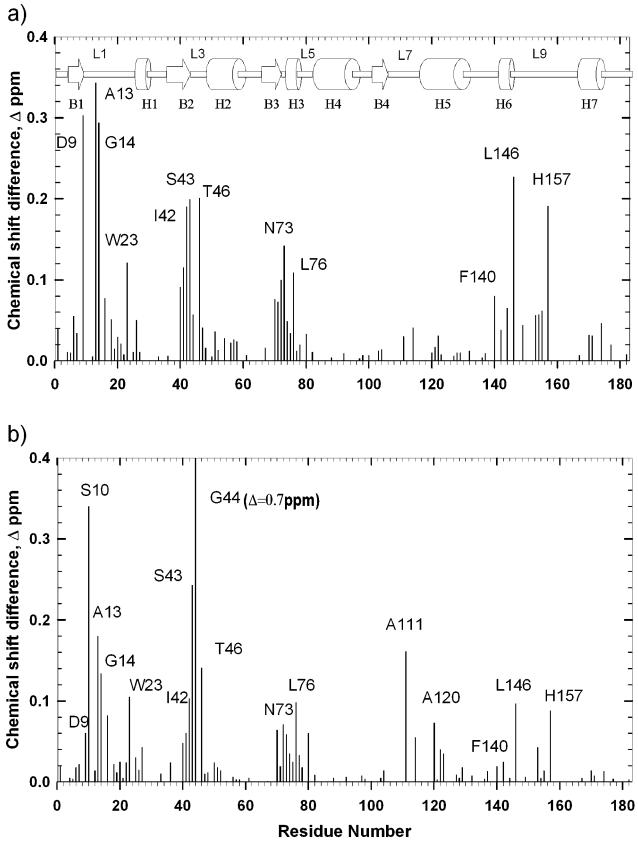

FIGURE 6: Sequence variation of chemical shift changes due to structural transitions. Chemical shift differences, Δ, were determined from ^{15}N-HSQC spectra of the corresponding samples obtained at 285 K. Chemical shift differences (a) between the free enzyme and the Michaelis complex and (b) between the Michaelis complex and the tetrahedral complex. The sequence locations of the secondary elements are shown on the top figure.

temperature employed for ESI-MS is likely to cause the conversion of some of the Michaelis complex into the tetrahedral covalent complex.

Thus, we can conclude that the intermediate species is the Michaelis complex and the final complex is the tetrahedral complex (structure II).

Mapping the Interaction Surface. As described above, under proper conditions MC can be trapped for a prolonged time for structural studies. Thus, we can compare the structural events that take place during the transition from the free enzyme to MC and from MC to the tetrahedral complex. Although the chemical shift dispersion in the ^{15}N-HSQC spectrum of TEP-I is excellent for its size, some spectral overlap is unavoidable, especially in the presence of several species at low temperature. To facilitate the resonance assignment, we prepared several samples with ^{15}N labeled at specific amino acids (alanine, leucine, and serine). We observed cross-peaks in the respective 2D ^{15}N-HSQC spectra for 18 out of 19 alanines, 23 out of 23 leucines, and 10 out of 11 serines (*18*). The excellent resolution in the ^{15}N-HSQC spectra makes it possible to unambiguously determine the chemical shift perturbations.

Figure 6 shows the composite amide ^{1}H and ^{15}N chemical shift differences between the free enzyme and the Michaelis complex (Figure 6a) and between the Michaelis complex and the tetrahedral complex (Figure 6b). The chemical shift differences are calculated using the expression $\Delta = [(\Delta\delta^2_{NH}$

$+ \Delta\delta^2_N/25)/2]^{1/2}$, where $\Delta\delta_{NH}$ and $\Delta\delta_N$ are the chemical shift differences for $^1H^N$ and ^{15}N, respectively (*34*). While one can expect positive correlation between the amount of chemical shift change and the degree of structural perturbation, the correlation, however, is not straightforward, and caution must be taken in interpreting the results. With the above understanding we can interpret our observation as follows: In both steps the residues involved appear to be localized in similar four loop segments: loop L1 region (Asp^9-Gly^{14}) which contains the catalytic Ser^{10}; loop L3 region ($Ala^{40}-Thr^{46}$); loop L5 region ($Leu^{70}-Leu^{76}$); and loop L9 region ($Phe^{140}-His^{157}$) which contains two catalytic residues, Asp^{154} and His^{157}. Together with loop L7 and helix H3 these segments make up the active site (*19*). All of the catalytic triad residues (Ser^{10}, Asp^{154}, and His^{157}) are perturbed, confirming that indeed DENP binds to the active site in a functionally relevant manner. Closer inspection of the details of the structural transitions reveals several interesting points: (1) Residues exhibit the largest shifts; namely, those located in loops L1 and L3 cluster around Ser^{10} while the residues around Asp^{154} show much less shift perturbation. Thus, DENP binds to a site near the Ser^{10}-O^γ group, as expected. (2) In the free enzyme the amide resonance of Ser^{10} cannot be detected, probably due to line broadening caused by conformational exchange (*19*). However, in MC a new resonance was observed in the ^{15}N-HSQC spectrum of the [U-^{15}N-Ser]TEP-I/DENP sample, and this resonance was assigned to Ser^{10}, since this is the only unassigned serine residue. Our ability to detect this resonance in the MC and tetrahedral complex states suggests that binding of DENP stabilizes the conformation of Ser^{10} or that binding causes the water exclusion from the binding pocket to reduce the line broadening of the Ser^{10} amide proton. (3) Transition from the MC to the tetrahedral complex was characterized by additional shifts in several resonances, the most prominent of which are Ser^{10}, Gly^{44}, and Ala^{111}. The large chemical shift change observed for Ser^{10} and Gly^{44} in the second step suggests the possibility of hydrogen bond formation between the phosphate group of DENP and $^1H^N$ of these groups, supporting the proposal that these two groups serve as the proton donors to the oxyanion. Thus, the present work represents the first direct experimental evidence for the formation of hydrogen bonds between the phosphate group of the transition state inhibitor and the oxyanion hole groups in solution. The observation of large chemical shift in residues Ala^{111} and Ala^{120} from loop 7, the most flexible loop in TEP-I (*19*), may indicate a large-scale movement of this loop at the second step.

DISCUSSION

Structural Transition upon Binding of DENP. The ribbon representations of the structure of TEP-I are shown in two views in Figure 7a,b (PDB ID: 1JRL). Asp^{154}, His^{157}, and Ser^{10} line up linearly on the side of a V-shape trough with the Asp^{154} residue near the surface and the Ser^{10} residue at the bottom of the trough. The active site is surrounded by loops L1, L3, L5, L7, and L9 and helix H3 (*19*). The two blue spheres are the putative oxyanion hole amide protons of Ser^{10} and GLy^{44}. The present study established that binding of DENP to TEP-I can be clearly divided into two steps: a rapid formation of the Michaelis complex followed by a slow conversion to the tetrahedral complex. The residues most affected in the first step are shown in Figure 7c. Those affected in the second step are shown in Figure 7d. Blue spheres in Figure 7c,d are the loci of amide groups with chemical shift change $\Delta \geq 0.1$ ppm, and the spheres colored cyan are residues with 0.1 ppm $> \Delta \geq 0.05$ ppm. In both steps the residues with the largest chemical shift perturbations are clearly localized around the Ser^{10} site. Interestingly, the residues affected the most appear to line up perpendicular to the line connecting the catalytic triad residues. On the basis of the present results we propose that the following structural events take place following DENP binding.

In the Michaelis complex DENP binds to the active site with the phosphate group already positioned near Ser^{10}, thus causing large chemical shift perturbations of the surrounding amide protons. Binding of DENP stabilizes the floppy Ser^{10} residue to adapt a defined conformation. Our previous studies have shown that the hydrogen bond between Asp^{154}-O^δ and His^{157}-$H^{\delta 1}$ is also perturbed at this step, as shown by perturbation of the low-field proton resonance assigned to His^{157}-$H^{\delta 1}$ (*30*). The observation of changes in $^1H^N$ resonances of Leu^{146} and His^{157} indicates structural changes in loop 9 at this step. Thus, residues perturbed at this step were confined mainly to the conserved segments comprising the binding pocket (L1, L3, H3, L5, and L9). The second step of conversion from the Michaelis complex to the tetrahedral complex involves the covalent binding of the phosphate group to Ser^{10}-O^γ. Residues affected at this step are located mostly in the same four conserved segments, suggesting a continuous adjustment of the active site geometry. Conversion of MC to the tetrahedral complex is further accompanied by the structure changes of the floppy loop L7 region, reflecting a possible further tightening up of the binding pocket. Thus, the prominent feature of the structural changes induced by DENP binding is the sequential structural rearrangement involving the four conserved segments.

Roles of the Conserved Residues in the SGNH Family of Proteins. In 1995, Upton and Buckley described a new family of lipolytic enzymes which share five consensus sequence blocks and which differ from other lipases in possessing a GDSLS motif, instead of the GxSxG motif (*15*). More recently, a subgroup of proteins within this family has been further classified as the SGNH-hydrolase due to the presence of four completely conserved residues: serine, glycine, asparagine, and histidine in blocks I, II, III, and V, respectively (*16*, *35*). Each of the four residues was proposed to play a central role in the catalytic function. The catalytic serine in block I serves as a nucleophile and a proton donor of the oxyanion hole. The glycine residue in block II and the asparagine in block III serve as two other proton donors to the oxyanion hole. The histidine residue in block V acts as a base to make Ser^{10} more nucleophilic by deprotonating the hydroxyl group. Sequence and structure comparisons have shown that TEP-I is also a member of the SGNH-hydrolase family (Lo and Liaw, unpublished observation). The corresponding four conserved residues in TEP-I are Ser^{10}, Gly^{44}, Asn^{73}, and His^{157}. The X-ray crystallographic structure of TEP-I in complex with diethyl phosphate (DEP) also showed that the amide proton of Ser^{10} and Gly^{44}, together with the H^δ of Asn^{73}, is positioned to serve as a proton donor in the oxyanion hole. The large chemical shift perturbations observed for the amide resonances of Ser^{10}, Gly^{44}, and Asn^{73} support the functionally important roles of

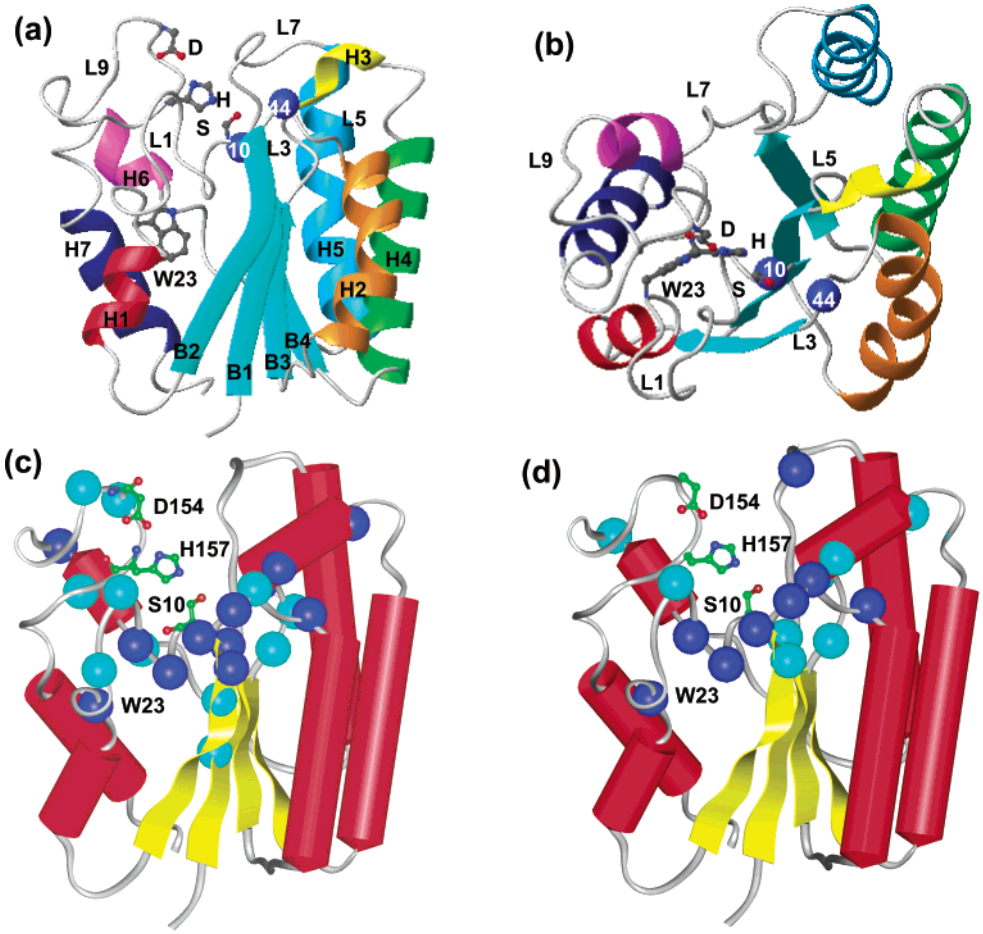

FIGURE 7: Schematic representation of the structure of TEP-I. (a) and (b) are two different orientations of free TEP-I. Helices are labeled as H1−H7, β strands as B1−B4, and loops as L1−L9. The two blue spheres are the two oxyanion hole residues Ser^{10}-H^N and Gly^{44}-H^N. (c) Residues perturbed due to structural transition from the free enzyme to the Michaelis complex. (d) Residues perturbed due to structural transition from the Michaelis complex to the tetrahedral complex. Spheres in (c) and (d) mark the locations of the amide protons with $\Delta \geq 0.1$ ppm (blue) or 0.1 ppm $> \Delta \geq 0.05$ ppm (cyan). Structures in (a), (c), and (d) are shown in the same orientation. (a) and (b) were prepared with the program MOLMOL (*44*), and (c) and (d) were prepared with the program InsightII (Accelrys).

these residues. The smaller chemical shift change in the amide resonance of Asn^{73} is consistent with the proposal that it is the H^{δ}, not the amide proton, which serves as the oxyanion acceptor. Mutation of Ser^{10} or His^{157} to Ala abolished the enzyme activity, confirming the catalytic roles of these two residues (Shaw et al., unpublished observations). Thus, our present study provides the first experimental evidence supporting the proposed functional roles of these strictly conserved residues in the SGNH-hydrolase family and confirms the location of the oxyanion hole as deduced from the X-ray crystallographic structure.

Hydrogen Bond Formation Involving the Oxyanion Hole Residues. Transition state theory postulates that enzymatic catalysis is due to the preferential binding of the substrate to the enzyme in a configuration that resembles the transition state complex (*2*, *4*, *36*). By doing so, the enzyme lowers the activation energy barrier of the reaction, resulting in an increase in reaction rate. The specific binding forces involved in distorting the scissile bond and stabilizing the transition state are provided by the hydrogen bonding between protein groups and the developing negative charge, the oxyanion on the substrate, in the oxyanion hole. In most serine proteases two peptide NH groups of the polypeptide backbone form the oxyanion hole. In subtilisin, the side chain H^{δ} of Asn^{155} is believed to provide one of the hydrogen-bonding groups in the oxyanion hole (*37*). Mutating Asn^{155} to Leu^{155} reduced k_{cat} by a factor of 200−300 (*38*). In a few serine hydrolases three oxyanion acceptors have been observed (*39*−*41*). In SGNH-hydrolases the oxyanion hole has three H-bond donors, and in TEP-I the three proton donors are the amide protons of Ser^{10} and Gly^{44} and the H^{δ} of Asn^{73}. Comparison of the structures of TEP-I and the TEP-I/DEP complex showed no change in the relative positions of the three proton donors to the oxyanion, suggesting that the oxyanion hole is preformed. How the oxyanion interacts with the proton donors has far-reaching consequences for the catalytic mechanism and is thus of considerable interest. In comparing the chemical shift changes at the two stages of DENP binding, as shown in Figures 6 and 7, we found that Asn^{73} changes more in the first step of MC formation. On the other hand, large shifts were observed for Ser^{10} and Gly^{44} in the second step of TC formation. The amount of chemical shift changes for Ser^{10} in the first step of MC formation cannot be determined since the amide resonance of Ser^{10} is not detectable in the free enzyme, probably due to fast exchange. Since hydrogen bond formation causes large chemical shifts, we postulate that the sequential change is due to the sequential formation of hydrogen bonds between the oxyanion, the phosphate group, and the respective proton donors. Thus, formation of the MC complex is accompanied by the

formation of a hydrogen bond between the phosphate group and the Asn^{73}-H^{δ}. The structure of the tetrahedral complex is further stabilized by two additional hydrogen bonds between the oxyanion and the amide groups of Ser^{10} and Gly^{44}. Thus, our results support a model in which DENP forms a hydrogen bond with Asn^{73}-H^{δ} in the MC. Formation of this H-bond may facilitate the nucleophilic attack of the phosphate group by Ser^{10}-O^{γ} to form the TEP-I/DEP TC which is stabilized by additional H-bonds between the oxyanion and the amide protons of Ser^{10} and Gly^{44}. The presence of H-bonds between the oxyanion and the proton donors is supported by the X-ray crystal structure at 2.0 Å resolution (Lo and Liaw, unpublished observations; PDB ID 1J00). It is interesting to note that the phosphodiester (structure II in Scheme 1) is electroneutral, which is not favorable for nucleophilic attack by Ser^{10}-O^{γ}. The presence of three proton donors, instead of two, in the oxyanion hole in TEP-I creates a positive environment to polarize the P═O bond, making the P═O phosphorus more electropositive and creating a partial negative charge at the oxygen to enhance the susceptibility of the phosphorus atom to nucleophilic attack by Ser^{10}-O^{γ}.

Role of Trp^{23}. It is interesting that Trp^{23} was also significantly affected in both steps. Moreover, the Trp^{23}-$H^{N\epsilon}$ resonance was shifted more than the backbone amide resonance during these two steps of binding (data not shown). Trp^{23} is located at the C-terminus of loop L1 and is over 10 Å away from the catalytic center (Figure 7a,b). Its side chain is located in the interior interface between the β sheet and helices H1, H6, and H7. Trp^{23} is likely to play an important structural role in stabilizing the interactions of the β sheet with the helices on one side, similar to that observed in other lipases (*42*, *43*). The large perturbation observed for Trp^{23} may indicate the presence of large-scale structural rearrangement in the interface region during catalysis. Since the catalytic Ser^{10} is attached to the β sheet while Asp^{154} and His^{157} are anchored on the loops connecting helices H6 and H9, the movement of Trp^{23} will definitely change the relative distances among the catalytic triad residues. Thus, we believe Trp^{23} is likely to play an important role in the catalytic process.

NOTE ADDED AFTER ASAP POSTING

This paper was inadvertently posted on the Web on 06/17/03 with the incorrect value given for the lifetime of transition states in the middle of the right-hand column on the first page. The correct version was posted 06/19/03.

REFERENCES

1. Eyring, H. (1935) *Chem. Rev. 17*, 65−77.
2. Pauline, L. (1946) *Chem. Eng. News 24*, 1375−1377.
3. Kurz, J. L. (1963) *J. Am. Chem. Soc. 85*, 987−991.
4. Schramm, V. L. (1998) *Annu. Rev. Biochem. 67*, 693−720.
5. Hammes, G. G. (1998) *Protein Sci. 7*, 799−802.
6. Wolfenden, R. (1969) *Nature 223*, 704−705.
7. Lolis., E., and Petsko, G. (1990) *Annu. Rev. Biochem. 59*, 597−630.
8. Wilmouth, R. C., Clifton, I. J., Robinson, C. V., Roach, P. L., Aplin, R. T., Westwood, N. J., Hajdu, J., and Schofield, C. J. (1997) *Nat. Struct. Biol. 4*, 456−462.
9. Wilmouth, R. C., Edman, K., Neutze, R., Wright, P. A., Clifton, I. J., Schneider, T. R., Schofield, C. J., and Hajdu, J. (2001) *Nat. Struct. Biol. 8*, 689−694.
10. Katona, G., Wilmouth, R. C., Wright, P. A., Berglund, G. I., Hajdu, J., Neutze, R., and Schofield, C. J. (2002) *J. Biol. Chem. 277*, 21962−21970.
11. Pacaud, M., and Uriel, J. (1971) *Eur. J Biochem. 23*, 435−442.
12. Cho, H., and Cronan, J. E., Jr. (1993) *J. Biol. Chem. 268*, 9238−9245.
13. Ichihara, S., Matsubara, Y., Kato, C., Akasaka, K., and Mizushima, S. (1993) *J. Bacteriol. 175*, 1032−1037.
14. Lee, Y. L., Chen, J. C., and Shaw, J. F. (1997) *Biochem. Biophys. Res. Commun. 231*, 452−456.
15. Upton, C., and Buckley, J. T. (1995) *Trends Biochem. Sci. 20*, 178−179.
16. Molgaard, A., Kauppinen, S., and Larsen, S. (2000) *Struct. Folding Des. 8*, 373−383.
17. Li, J., Derewenda, U., Dauter, Z., Smith, S., and Derewenda, Z. S. (2000) *Nat. Struct. Biol. 7*, 555−559.
18. Lin, T. H., Chen, C. P., Huang, R. F., Lee, Y. L., Shaw, J. F., and Huang, T. H. (1998) *J. Biomol. NMR 11*, 363−380.
19. Huang, Y. T., Liaw, Y. C., Gorbatyuk, V. Y., and Huang, T.-h. (2001) *J. Mol. Biol. 307*, 1075−1090.
20. Cohen, J. A., Oosterbaan, R. A., and Berends, F. (1967) *Methods Enzymol. 11*, 686−702.
21. Massiah, M. A., Viragh, C., Reddy, P. M., Kovach, I. M., Johnson, J., Rosenberry, T. L., and Mildvan, A. S. (2001) *Biochemistry 40*, 5682−5690.
22. Lee, Y. L., Su, M. S., Huang, T. H., and Shaw, J. F. (1999) *J. Am. Oil Chem. Soc. 76*, 1113−1118.
23. Gill, S., and von Hippel, P. (1989) *Anal. Biochem. 182*, 319−326.
24. Rua, M. L., Diaz-Maurino, T., Fernandez, V. M., Otero, C., and Ballesteros, A. (1993) *Biochim. Biophys. Acta 1156*, 181−189.
25. Barnes, E. M., Jr., and Wakil, S. J. (1968) *J. Biol. Chem. 243*, 2955−2962.
26. Piotto, M., Saudek, V., and Sklenar, V. (1992) *J. Biomol. NMR 2*, 661−665.
27. Wishart, D. S., and Sykes, B. D. (1994) *Methods Enzymol. 239*, 363−392.
28. Wishart, D. S., Bigam, C. G., Yao, J., Abildgaard, F., Dyson, H. J., Oldfield, E., Markley, J. L., and Sykes, B. D. (1995) *J. Biomol. NMR 6*, 135−140.
29. Neidig, K. P., Geyer, M., Gorler, A., Antz, C., Saffrich, R., Beneicke, W., and Kalbitzer, H. R. (1995) *J. Biomol. NMR 6*, 255−270.
30. Tyukhtenko, S. I., Litvinchuk, A. V., Chang, C. F., Leu, R. J., Shaw, J. F., and Huang, T.-h. (2002) *FEBS Lett. 528*, 203−206.
31. Millard, C., Koellner, G., Ordentlich, A., Shafferman, A., Silman, I., and Sussman, J. (1999) *J. Am. Chem. Soc. 121*, 9883−9884.
32. Viragh, C., Harris, T. K., Reddy, P. M., Massiah, M. A., Mildvan, A. S., and Kovach, I. M. (2000) *Biochemistry 39*, 16200−16205.
33. Douglas, D. J., Collings, B. A., Numao, S., and Nesatyv, V. J. (2001) *Rapid Commun. Mass Spectrom. 15*, 89−96.
34. Grzesiek, S., Stahl, S. J., Wingfield, P. T., and Bax, A. (1996) *Biochemistry 35*, 10256−10261.
35. Dalrymple, B., Cybinski, D., Layton, I., McSweeney, C., Xue, G., Swadling, Y., and Lowry, J. (1997) *Microbiology 143*, 2605−2614.
36. Pauline, L. (1948) *Am. Sci. 36*, 50−58.
37. Robertus, J. D., Kraut, J., Alden, R. A., and Birktoft, J. J. (1972) *Biochemistry 11*, 4293−4303.
38. Bryan, P., Pantoliano, W., Quill, S. G., Hsiao, H.-Y., and Poulos, T. (1986) *Proc. Natl. Acad. Sci. U.S.A. 83*, 3743−3745.
39. Grochulski, P., Bouthillier, F., Kazlauskas, R. J., Serriqi, A. N., Schrag, J. D., Ziomek, E., and Cygler, M. (1994) *Biochemistry 33*, 3494−3500.
40. Nicolas, A., Egmond, M., Verrips, C. T., de Vlieg, J., Longhi, S., Cambillau, C., and Martinez, C. (1996) *Biochemistry 35*, 398−410.
41. Ordentlich, A., Barak, D., Kronman, C., Ariel, N., Segall, Y., Velan, B., and Shafferman, A. (1998) *J. Biol. Chem. 273*, 19509−19517.
42. Chiba, H., Histanke, M., Hirose, M., and Sugimoto, E. (1973) *Biochim. Biophys. Acta 327*, 380−392.
43. Liu, W. H., Beppu, T., and Arima, K. (1977) *Agric. Biol. Chem. 41*, 131−135.
44. Koradi, R., Billeter, M., and Wuthrich, K. (1996) *J. Mol. Graphics 14*, 51−55.

BI027246W